CHAPTER 4

Results and Discussion

The numerical and experiment results will be discussed in this chapter. The first part is the ORC numerical simulation analysis of the computer software as a Microsoft Excel. The second part demonstrates the experimental results and the discussion on the characteristics of the temperature, pressure, torque and power output. The third part the discussion on the irreversibility on the ORC system. The last part is verification of the numerical and experimental ORC system.

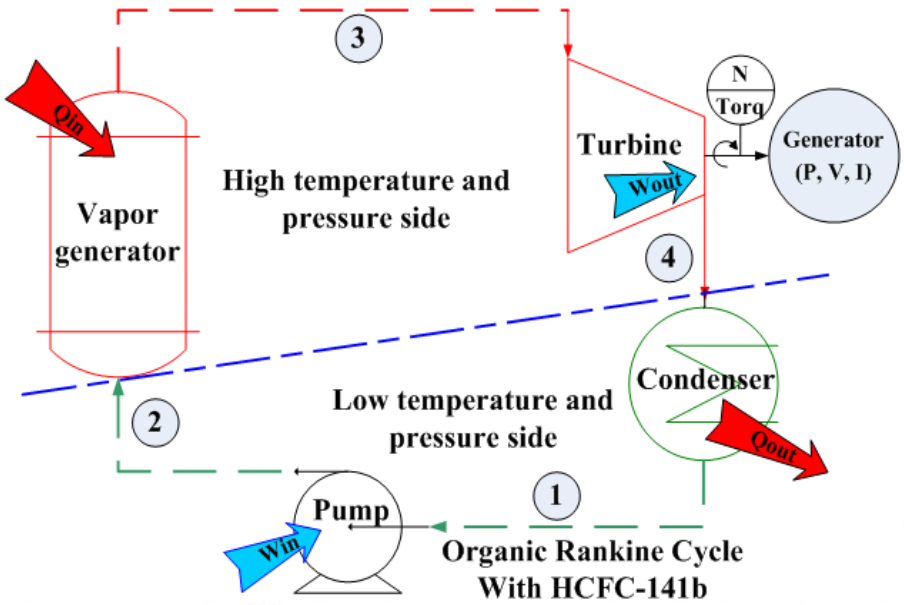

Copyright© by Chiang Mai University
All rights reserved

Figure 4.1: Schematic diagram of ORC for numerical simulation

Figure 4.1 shows the diagram and points of analysis and experimental measurement in the study purpose, whereas the nomenclature positions are correspondent to the experimental rig. The numerical simulations were operated and simulation of the system performed to gain informations upon which based upon comparative results gained from improves parameter using numerical simulation. It should be noted that the method used to heat source temperature in the system had a limited range of heating rates. As a

consequence, the rate was set to provide the heat transfer into the vapor generator without taking the pressure differential of the rig above its maximum. For all of the trials conducted, the working fluid mass flow rate was set to the maximum limit to be provided to the rig.

4.1 ORC Numerical Simulations

The results of simulation can be descriped that the effects of the heat rate of vapor generator and the turbine work output as a function the heat source temperature in the case of working fluid mass flow rate 372 kg/h, while the heat source temperature input at the vapor generator are varie between 70 - 100^{o}C. The heat rate of vapor generator and the turbine work output increases corresponding to the incresing of the heat source temperature.

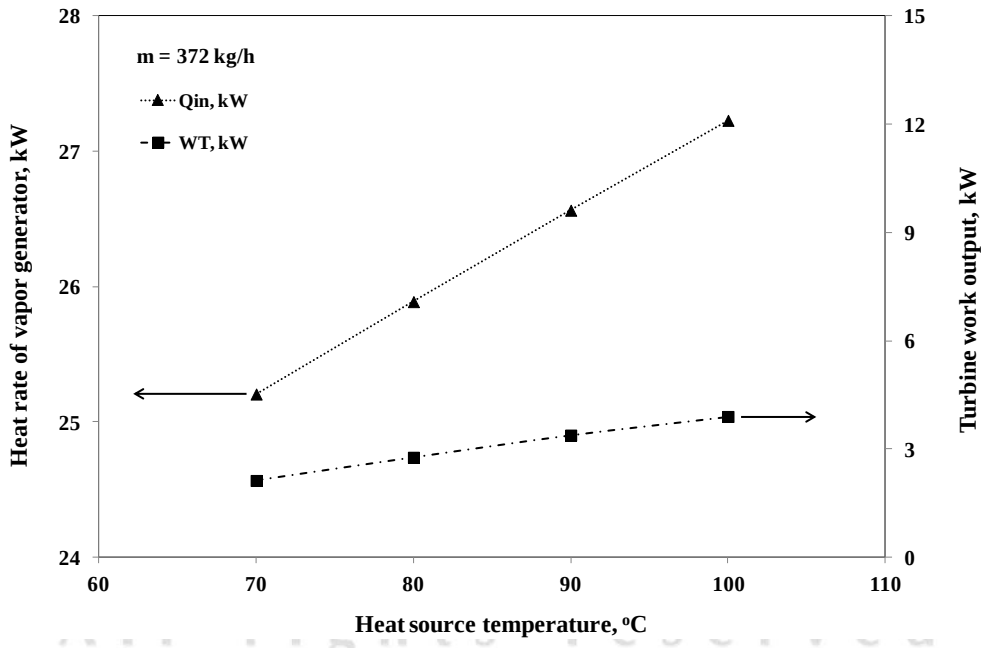

Figure 4.2: Effects of heat rate of vapor generator and turbine work output on heat source temperature at mass flow rate setting 372 kg/h

Figure 4.2 can be concluded that, the heat rate of vapor generator and turbine work output should be able to rise as the heat source temperature increases. It is therefore obviously apperared that the turbine work output and heat rate of vapor

generator increases when heat source temperature increases. It can be concluded that if working fluid with a low latent heat is used the saturated or superheat vapor at the turbine work output would give the good performance and good operating conditions.

Table 4.1 shows the numerical simulation results, the working fluid mass flow rates were presetted between 112 - 372 kg/h (0.031 – 0.103 kg/s) and the heat source temperature was 100°C. The theoretical turbine work output results were between 1.2 - 3.9 kW, whereas the thermal efficiency for the heat source temperature was shown in Table 4.1. All cases of the heat source temperature was fixed at 100°C, the system offered the Rankine cycle efficiency in the range between 14.1 - 14.2% and the Carnot cycle efficiency is 16.5%.

Table 4.1: Numerical simulation on heat source temperature set at 100°C

Parameters	Unit	Numerical simulation results			
		Input conditions			
m_{wf}	kg/h	112	223	298	372
T_{so}	°C	100	100	100	100
$T_{vg,wf,i}$	°C	30.3	30.3	30.3	30.3
$T_{vg,wf,o}$	°C	90	90	90	90
$P_{vg,wf,o}$	kPa	538	538	538	538
$T_{T,o}$	°C	33	33	33	33
$P_{T,o}$	kPa	105	105	105	105
Pr	-	5	5	5	5
		Calculation results			
Q_{vg}	kW	8.2	16.4	21.8	27.3
Q_{co}	kW	7.0	14.0	18.7	23.4
W_t	kW	1.2	2.4	3.2	3.9
W_p	kW	0.01	0.02	0.03	0.04
W_{net}	kW	1.2	2.3	3.1	3.9
η_R	%	14.1	14.2	14.2	14.2
η_C	%	16.5	16.5	16.5	16.5

ลิขสิทธิ์มหาวิทยาลัยเชียงใหม่
Copyright© by Chiang Mai University
All rights reserved

Figure 4.3 shows the effects of the heat rejection at condenser and net power output on the working fluid mass flow rate varied between 112 - 372 kg/h (0.031 – 0.103 kg/s) and heat source temperature is set at 100ºC. The results shown that the heat rejection of condenser and net power output increased as the working fluid mass flow rate increases, consequently the system offer a higher net power output. Therefore rising of the working fluid mass flow rate of using HCFC-141b give good net power output as well as the better system performance. Further calculation offer that the net power output and heat rejection of condenser of the system are between 2.1 kW up to 3.9 kW and 7.0 kW up to 23.3 kW, respectively. The simulation results show that increasing of mass flow rate from the calculating has not yet the predicted effect of bringing the power output to the numerical calculation as that clarly shown the trend in Figure 4.3.

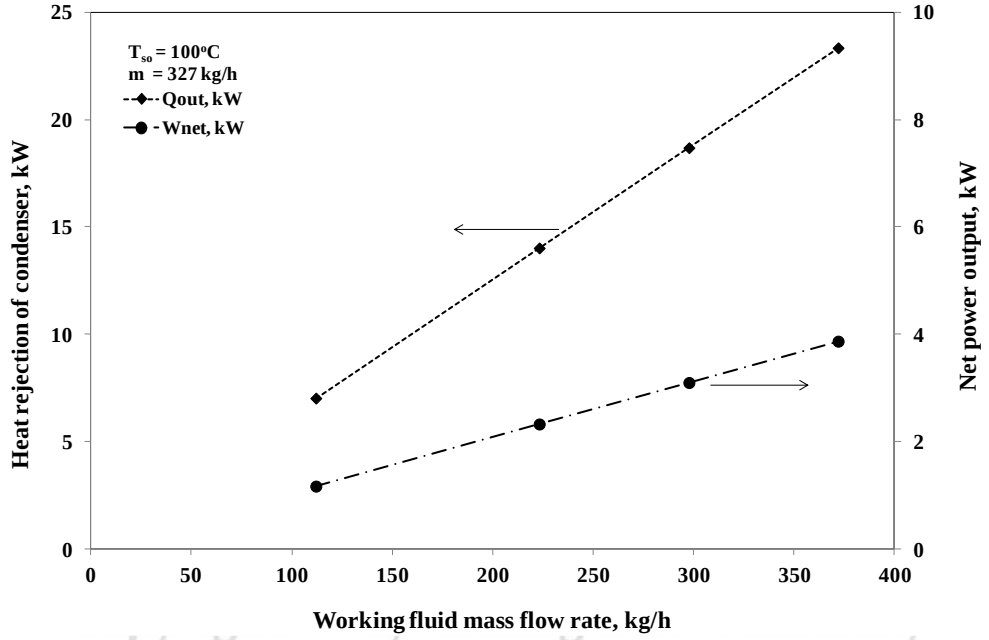

All rights reserved

Figure 4.3: Effects of working fluid mass flow rate on heat rejection of condenser and net power output in case of heat source temperature 100ºC

Figure 4.4 and 4.5, shows the relationship the turbine work output and cycle efficiency on the turbine inlet temperature of the heat source temperature difference between 70 – 100°C and all case of working fluid mass flow rate varied 112 - 372 kg/h (0.031 – 0.103 kg/s), respectively. These results shown that the characteristics of that

increasing the turbine inlet temperature, can improve not only the turbine outlet temperature but also increasing the overall cycle efficiency of the system.

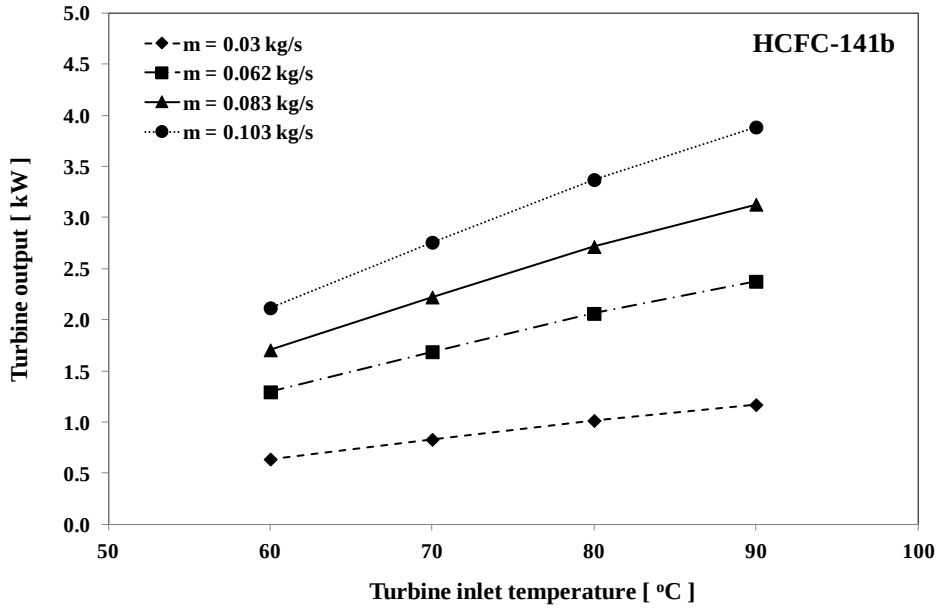

Figure 4.4: Relationship between turbine outputs on turbine inlet temperatures

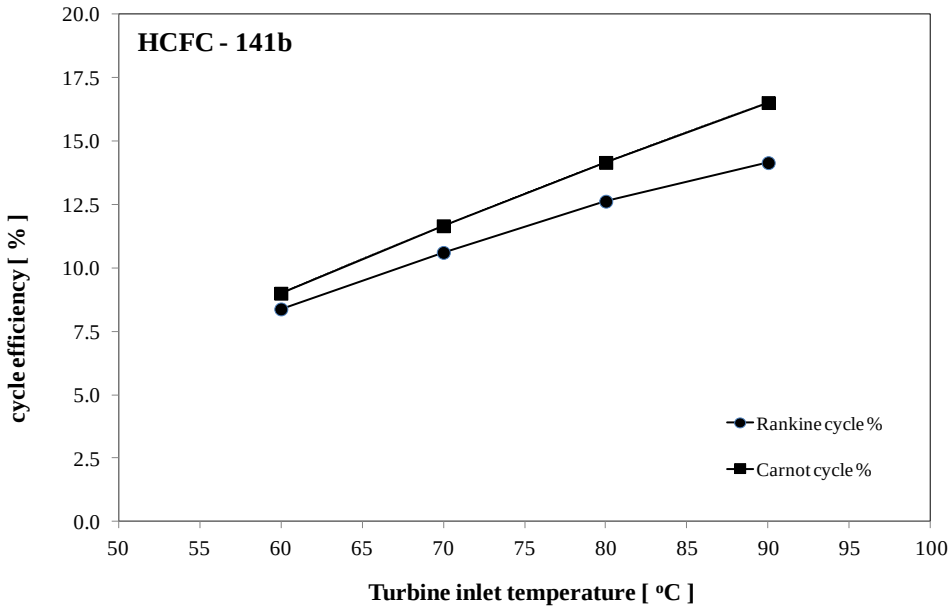

Figure 4.5: Relationship between turbine inlet temperatures on cycle efficiency

4.2 Characteristic of ORC System

4.2.1 Effects of Vapor Generator Temperature on Heat Source Temperature

The experimental result of the heat source temperature upon the vapor generator outlet temperature is shown in Figure 4.6.

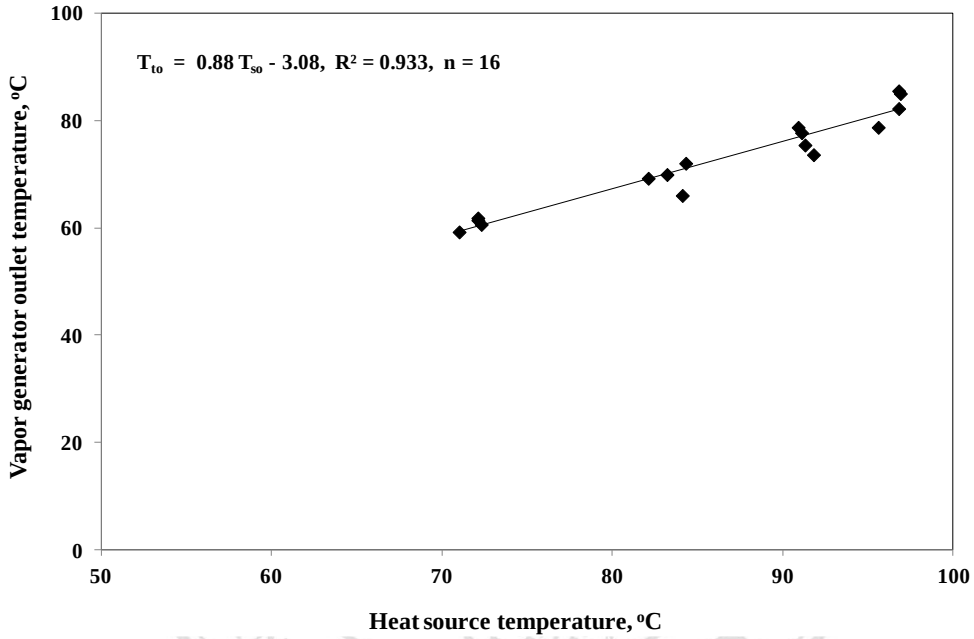

Figure 4.6: Effects of vapor generator outlet temperature on heat source temperature

ลิขสิทธิ์มหาวิทยาลัยเชียงใหม่
Copyright© by Chiang Mai University
All rights reserved

Figure 4.6 can be described that when increased heat source temperature cause's direct effect to an increased vapor generator outlet temperature, therefor operating conditions should be operated at the highest heat source temperature as the vapor generator heat rate input increased. In the case of a maximum heat source temperature was 96.9°C and working fluid mass flow rate was 391.7 kg/h causes the outlet temperature at vapor generator was 81.6°C. Whereas the minimum heat source temperature was 72.6°C and working fluid mass flow rate was 126.0 kg/h, the outlet temperature at the vapor generator was 61.1°C. The fixed temperature differential between the vapor generator and heat source makes predicting the outcome for the prototype ORC when it is operating at its maximum heat input rate.

4.2.2 Proportion of Pressure on Temperature at Vapor Generator

In this section considered the proportion of the temperature up on the pressure at the vapor generator outlet condition. For sixteen experiments cases, there is an optimum operating conditions to a highly heat source temperature as the vapor generator heat rate input increased.

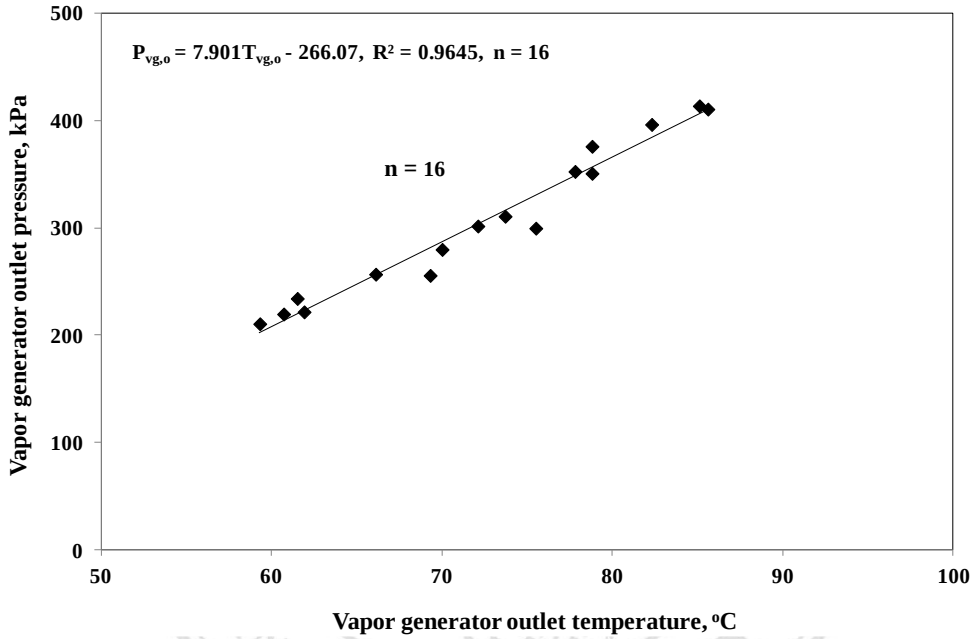

Figure 4.7: Relationship between temperature and pressure on vapor generator outlet

In the Figure 4.7, shows that when increased heat source temperature cause's effect to an increased vapor generator outlet temperature, therefor operating conditions should be operated at the outlet pressure of vapor generator increased as the vapor generator heat rate input increased. In the case of a maximum heat source temperature and working fluid mass flow rate testing condition were 96.9°C and 391.7 kg/h, the outlet temperature and pressure at vapor generator were 81.6°C and 446.5 kPa, repectively. Whereas the minimum heat source temperature and working fluid mass flow rate were 72.6°C and 126.0 kg/h, the outlet temperature and pressure at the vapor generator were 61.1°C and 236.5 kPa, respectively.

ลิขสิทธิ์มหาวิทยาลัยเชียงใหม่
Copyright© by Chiang Mai University
All rights reserved

4.2.3 Maximum Power Output on Heat Source Temperature

Table 4.2 shows the maximum power output conditions on the heat source temperature were 96.1, 96.8, 95.6, and 96.8^{o}C, the maximum power output were 1.6, 4.4, 12.5, and 15.7 W, while the theoretical power output were 1.2, 2.4, 3.1, and 3.9 kW, respectively. The thermal efficiency of system for the heat source temperature in the Table 4.2, the case of heat source temperature was 96.8^{o}C the measured system efficiency was 0.07%, while the Carnot cycle efficiency was 14.2%. It can be seen that experimental efficiency is very less than of the theoretical efficiency.

Table 4.2: Maximum power output on high temperature heat source condition

Parameter	Unit	Maximum power output condition			
T_{so}	^{o}C	96.1	96.8	95.6	96.8
m_{wf}	kg/h	128.9	239.1	305.5	384.4
$T_{vg,wf,i}$	^{o}C	31.8	30.7	33.4	31.7
$P_{vg,wf,o}$	kPa	478	484	398	397
$T_{vg,wf,o}$	^{o}C	85.1	85.6	77.8	82.3
$Q_{vg,i}$	kW	8.4	15.8	17.3	23.7
Pr	-	1.15	1.18	1.13	1.13
N	rpm	573	946	1,420	1,369
t	N.m	0.023	0.044	0.084	0.110
$p_{T,max}$	W	1.6	4.4	12.5	15.7
η_{sys}	%	0.02	0.03	0.07	0.07
η_{cnt}	%	14.8	15.1	13.2	14.2

ลิขสิทธิ์มหาวิทยาลัยเชียงใหม่
Copyright© by Chiang Mai University
All rights reserved

4.2.4 Maximum Power Output on Turbine Torque

Figure 4.8 shows the relationship of maximum power output on the turbine torque in the sixteen experiments. These results operated at the system keeping that the vapor generator temperature was set constant. For all the power output, the system efficiency increases linearly with the increase in turbine torque.

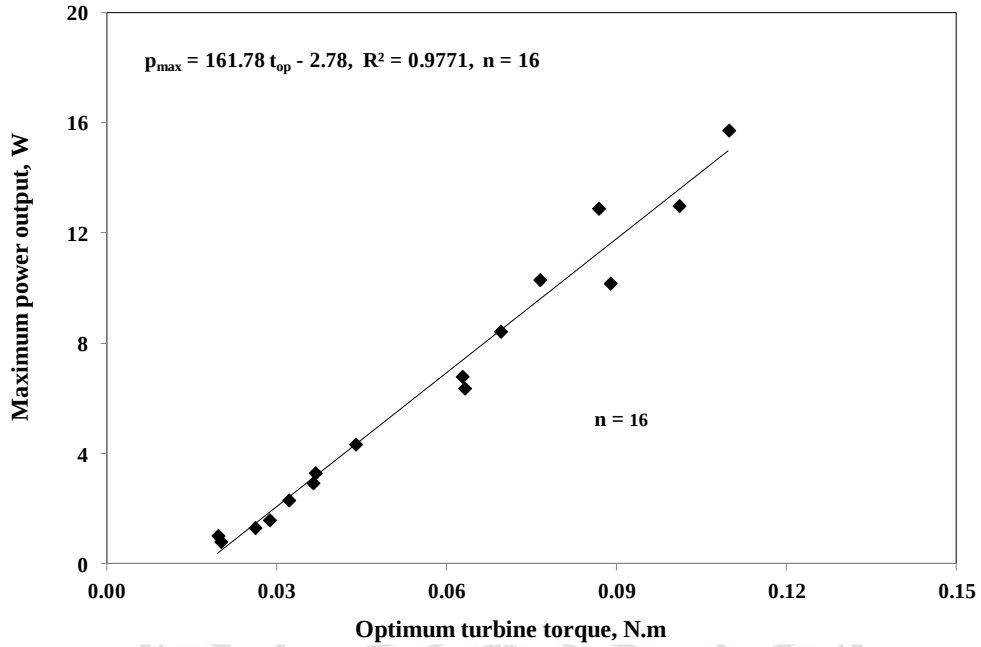

Figure 4.8: Relationship maximum power output on turbine torque

The optimum turbine torque and maximum power output at the optimum condition will be proportional increased was caused by heat source temperature and working fluid mass flow rate increased between the vapor generator and the pressure difference at turbine process. The results can be developed optimum equation of the system as expressed by Equation 4.1 with the coefficient of determination (R^2) of 97.71%.

$$p_{max} = 161.78t^2 - 2.7765 \qquad (0.02 < t < 0.11,\ R^2 = 0.9771,\ n = 16) \qquad 4.1$$

Where p_{max} is the maximum power output, W

t is the turbine torque, N.m

4.2.5 Effects of Turbine Torque and Power Output on Temperature Differences at Turbine

Figure 4.9 and 4.10 shown the effects of turbine torque and power output when the turbine inlet and outlet temperature difference between 2 - 6^{o}C as a function of heat source temperature and working fluid mass flow rate.

ลิขสิทธิ์มหาวิทยาลัยเชียงใหม่
Copyright© by Chiang Mai University
All rights reserved

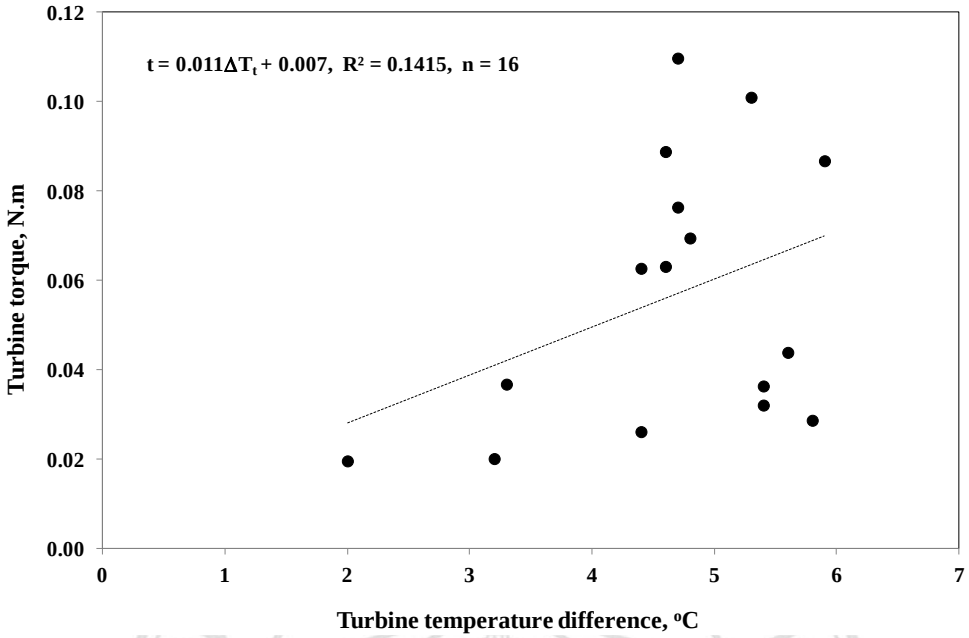

Figure 4.9: Effects of turbine torque on turbine temperature difference

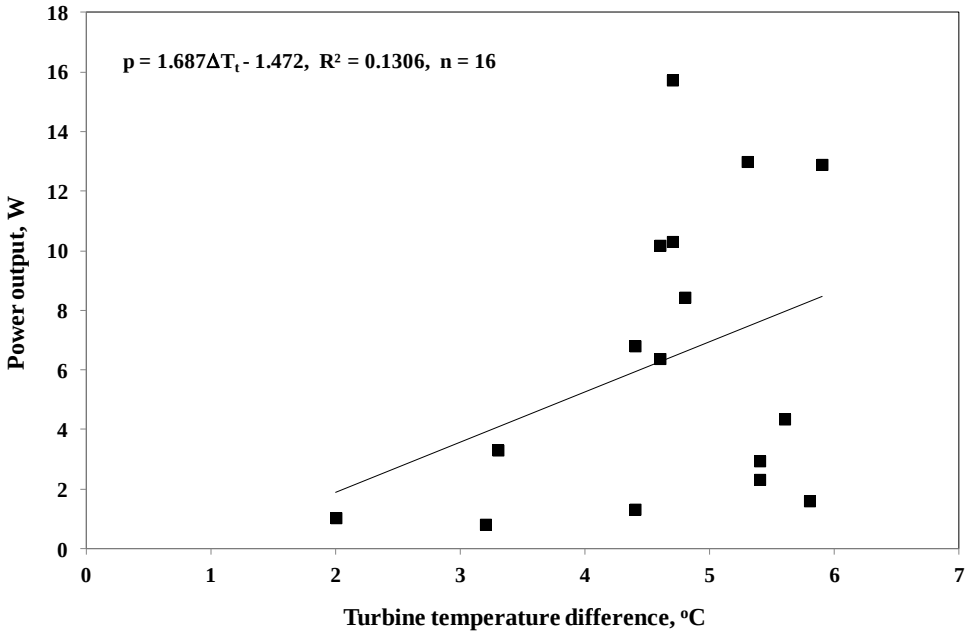

Figure 4.10: Effects of power output on turbine temperature difference

The temperature difference on the turbine process increased will be has the torque and power of turbine increased as heat sources temperature increased. The experiment

all case, the optimum condition when temperature difference was 4.7°C at the working fluid mass flow rate 378.1 kg/h and heat source temperature 96.8°C, the turbine torque and power output reached 0.11 N.m and 15.7 W, respectively. Therefore the turbine torque and power output increment was caused by temperature difference across turbine state conducted to kinetic energy on turbine blade and converted to shaft power.

4.2.6 Characteristic of Turbine Torque on Turbine Rotation Speed

Figure 4.11 and 4.12 shows the characteristic of turbine torque and average turbine torque as a function of turbine rotation speed. The rotation speed increased with the diminishing of the turbine torque. Whereas the overall turbine torque will be increased as heat sources temperature increased but rotation speed to be increased as torque will be decreased to stop. In the case of maximum heat source temperature was 96.1°C, the maximum turbine torque and average turbine torque reached 0.03 N.m and 0.02 N.m, respectively; similar results were obtained the cases of heat source temperature were 72.4, 82.3, and 90.7°C (Detail of calculation is complied in Appendix A).

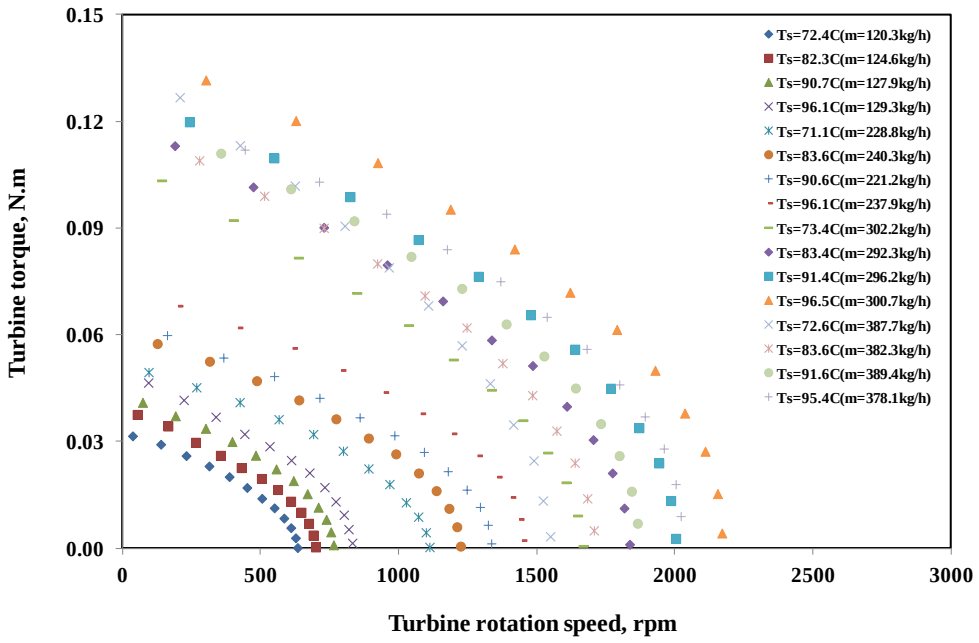

Figure 4.11: Characteristic of turbine torque on turbine rotation speed

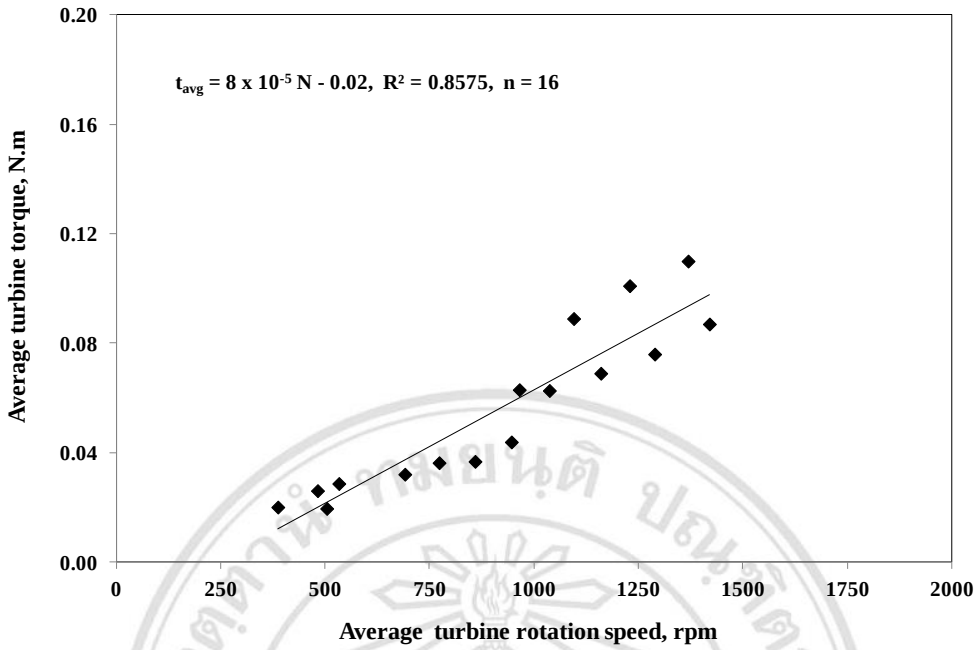

Figure 4.12: Relationship of average turbine torque on turbine rotation speed

The torque of experiment will be increment was caused by pressure difference between the turbine inlet and outlet. The results can be developing turbine torque equation of the ORC system as Equation 4.2 with the coefficient of determination (R^2) of 85.8%.

$$t = 8x10^{-5} N^2 - 0.02 \quad (0 < N < 1{,}500) \qquad 4.2$$

Where t is the turbine torque, N.m

N is the turbine rotation speed, rpm

ลิขสิทธิ์มหาวิทยาลัยเชียงใหม่
Copyright© by Chiang Mai University
All rights reserved

4.2.7 Characteristic of Power Output on Turbine Rotation Speed

Figure 4.13 and 4.14 shows the characteristic of power output and average power output of each experiment as a function of turbine rotation speed. The turbine rotation speed increased will be the power output rised to the maximum power and decreased to turbine rotation speed stopped but average power output will be increased as heat sources temperature increased but rotation speed to be increased as power will be decreased to stop. In the case of the heat source temperature was 96.1^{o}C, the

maximum power output and average power output reached 1.6 W and 1.1 W, respectively; similar results were obtained the cases of heat source temperature were 72.4, 82.3, and 90.7^{o}C (Detail of calculation is complied in Appendix A).

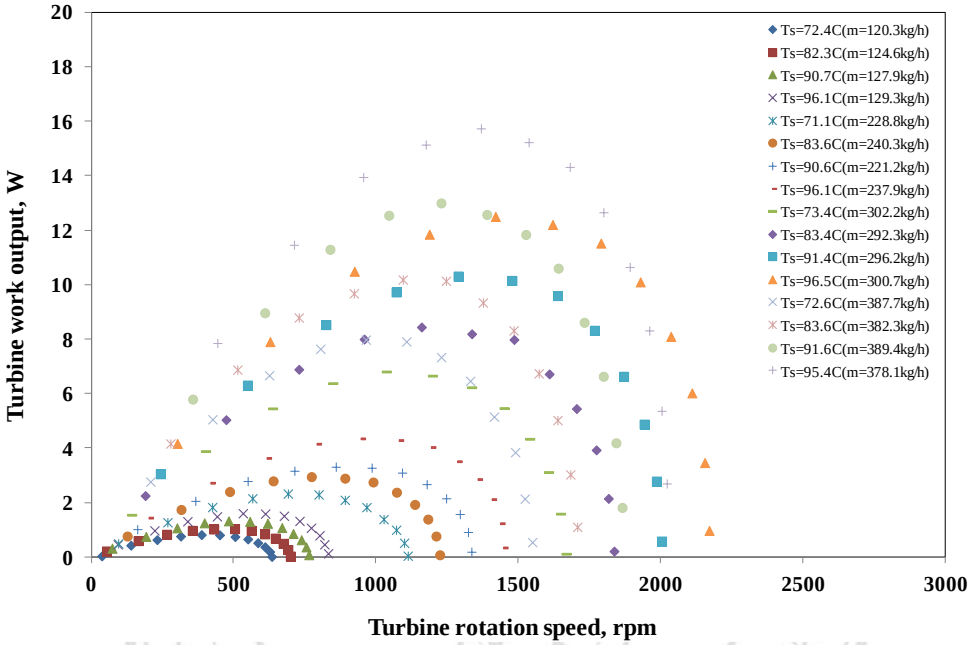

Figure 4.13: Characteristic of power output and turbine rotation speed

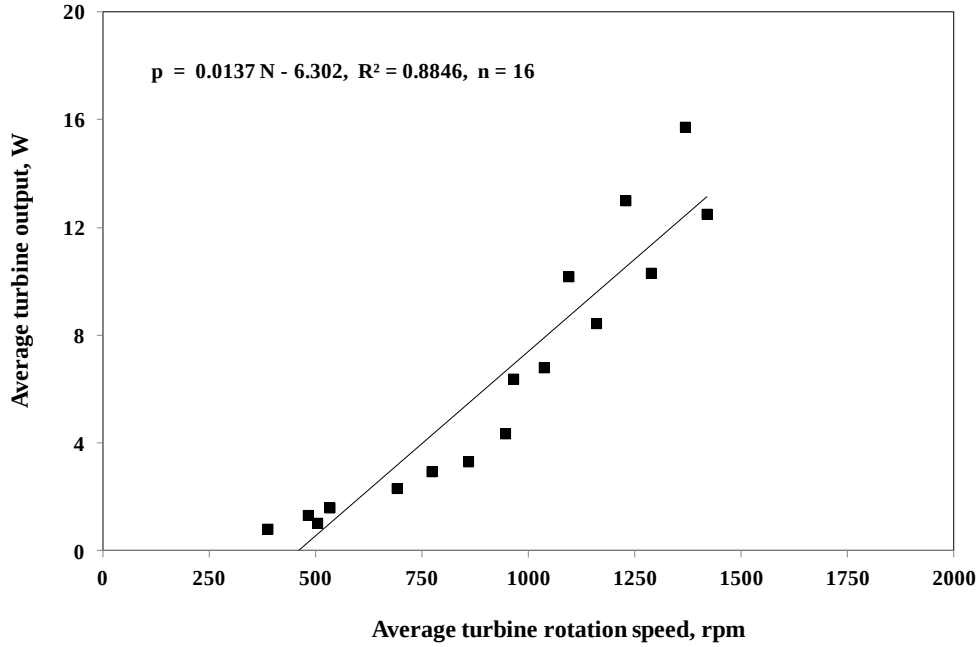

Figure 4.14: Effects of average power output on turbine rotation speed

The maximum power output increment was caused by pressure drop between the turbine inlet and outlet in the case of test rig system. The results can be developing power equation of ORC system as expressed by Equation 4.3 with the coeeficient of determination (R^2) of 88.5%.

$$p = 0.0137\,N + 6.302 \quad (0 < N < 1{,}500) \qquad 4.3$$

Where p is the turbine power output, W

N is the turbine rotation speed, rpm

4.2.8 Effects of Turbine Torque and Power Output on Working Fluid Mass Flow Rates

Figure 4.15 shows the characteristic of turbine torque and power output as a function of working fluid mass flow rate when the heat source temperature between 72.4°C to 96.1°C. The working fluid mass flow rate increased will be the turbine torque and power output increased as temperature heat sources increased. The heat source temperature was 96.1°C the maximum torque and power output reached 0.047 N.m and 1.60 W, respectively; similar results were obtained the cases of heat source temperature were 72.4, 82.3, and 90.7°C.

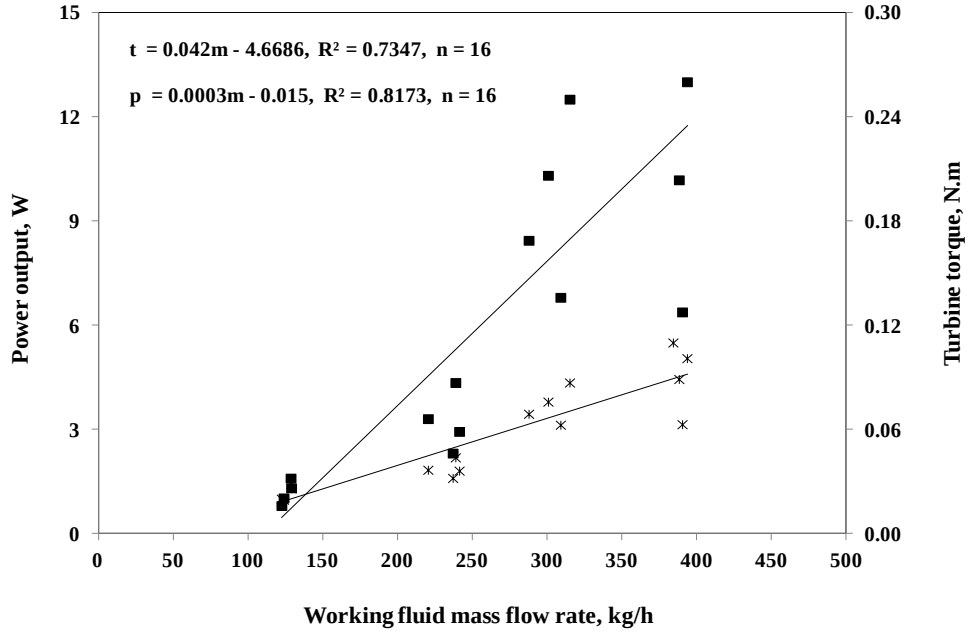

Figure 4.15: Effects of turbine torque and power output on working fluid mass flow rate

The power output change was caused by pressure difference between the turbine inlet and outlet. The results can be developing optimum equation of system as expressed by Equation 4.4 and 4.5 with the coefficient of determination (R^2) of 73.5% and 81.7% respectively.

$$t = 0.042\dot{m}_{wf} - 4.67 \quad (0 < N < 1{,}500) \tag{4.4}$$

and

$$p = 0.0003\dot{m}_{wf} - 0.02 \quad (0 < N < 1{,}500) \tag{4.5}$$

where p is the power output, W

t is the turbine torque, N.m

$\dot{m}_{wf}$ is the working fluid mass flow rate, kg/h

4.2.9 Optimum Condition of ORC System

The efficiency of the turbine varies from a highly of 0.07% down to 0.0163% with an all experiment. This falls far short of the design efficiency. Hence reducing the working fluid mass flow rate exit from the original testing has not had the predicted effect of bringing the power output of the turbine up to the design output. Reasons for predicted power were examined in Figure 4.15, 4.16 and Table 4.3.

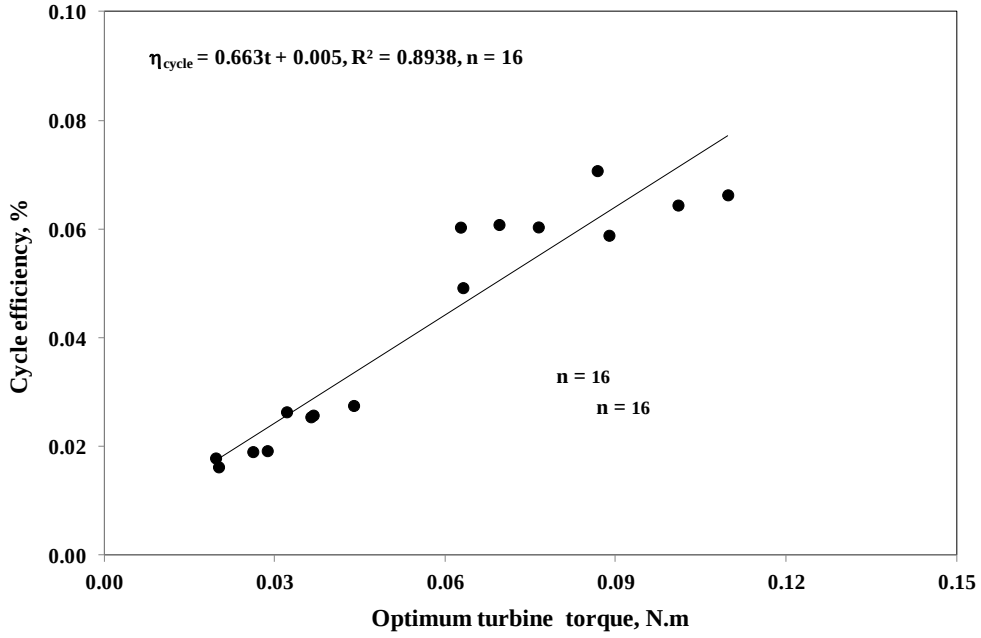

Figure 4.16: Cycle efficiency on optimum turbine torque

Table 4.3: Optimum operating condition of ORC test rig

No. of test	Code of test	Optimum torque (N.m)	Maximum power output (W)	ORC efficiency (%)
1	A-150613	0.0201	0.81	0.0163
2	B-160613	0.0196	1.03	0.0179
3	C-220613	0.0261	1.32	0.0191
4	D-230613	0.0287	1.60	0.0192
5	E-300613	0.0321	2.32	0.0264
6	F-060713	0.0363	2.94	0.0255
7	G-070713	0.0368	3.31	0.0258
8	H-130713	0.0439	4.35	0.0275
9	I-140713	0.0627	6.80	0.0604
10	J-200713	0.0695	8.44	0.0608
11	K-210713	0.0764	10.31	0.0604
12	L-260713	0.0868	12.90	0.0707
13	M-270713	0.0631	6.38	0.0492
14	N-030813	0.0888	10.18	0.0589
15	O-040813	0.1010	13.00	0.0644
16	P-090813	0.1097	15.73	0.0663

The ORC efficiency can be developing equation as a fuction of optimum torque condition of system and expressed by Equation 4.6 with the coefficient of determination (R^2) of 89.4%.

$$\eta_{cycle} = 0.663t - 0.005 \qquad (0 < N < 1{,}500) \qquad 4.6$$

ลิขสิทธิ์มหาวิทยาลัยเชียงใหม่
Copyright© by Chiang Mai University
All rights reserved

where η is the cycle efficiency

t is the turbine torque, N.m

$\dot{m}_{wf}$ is the working fluid mass flow rate, kg/h

4.3 Irreversibility Analysis

4.3.1 Effects of Irreversibility on ORC System

The effects investigate of the performance on the ORC system irreversible and second law efficiency the following operating conditions was used. The forth working fluid mass flow rates varied 120.3 – 387.7 kg/h with difference heat source temperature ranging from 72.1 – 96.8ºC was considered. The methodology is called an available work or the exergy method. A flow process diagram in Figure 4.1 with the different steps involved to apply the method was presented in Table 4.4. In addition, an exergy table of the entire process is represented using the pie graph.

Table 4.4: Total exergy rates with heat source temperature on ORC test rig

No. exp	T_{so} (ºC)	I_p (kW)	I_{vg} (kW)	I_T (kW)	I_C (kW)	I_{Total} (kW)
A-150613	72.1	0.232	1.544	0.069	1.037	2.881
B-160613	82.1	0.236	1.964	0.041	6.911	9.152
C-220613	91.3	0.236	2.486	0.107	3.415	6.244
D-230613	96.9	0.237	3.025	0.118	1.732	5.112
E-300613	72.1	0.295	2.876	0.225	1.866	5.262
F-060713	83.2	0.294	3.934	0.221	13.322	17.770
G-070713	90.9	0.295	4.511	0.094	12.065	16.964
H-130713	96.8	0.295	5.696	0.209	3.195	9.395
I-140713	72.3	0.353	3.664	0.236	16.485	20.737
J-200713	84.3	0.357	4.836	0.226	2.982	8.400
K-210713	91.1	0.354	6.036	0.224	3.450	10.064
L-260713	95.6	0.354	6.619	0.294	3.645	10.913
M-270713	71.0	0.416	4.310	0.316	2.877	7.918
N-030813	84.1	0.410	5.895	0.301	3.545	10.150
O-040813	91.8	0.414	7.268	0.337	20.861	28.881
P-090813	96.8	0.414	8.638	0.277	4.888	14.216

ลิขสิทธิ์มหาวิทยาลัยเชียงใหม่
All rights reserved

4.3.2 Effect of Turbine Exergy Destruction on Working Fluid Mass Flow Rate

The effects of turbine exergy destruction with the working fluid mass flow rate on the system were given in Figure 4.17. It can be shown that the total system turbine exergy destruction increases with working fluid mass flow rate and heat source temperature increased. The results illustrated in this figure the importance of performing a second law analysis. According to the results the cycle efficiency is approximately

decrease with the increment of the turbine exergy destruction increased. However, from a combined first and second law analysis, the best case scenario is obtained when the system was operated at superheated or saturated conditions before the turbine. This yields the same cycle efficiency with lower exergy destruction than operating under saturated or superheated conditions. In Figure show that the system with higher (m = 327.0 kg/h) and lower (m = 112.0 kg/h) of working fluid mass flow rate as a fuction of turbine exergy destruction.

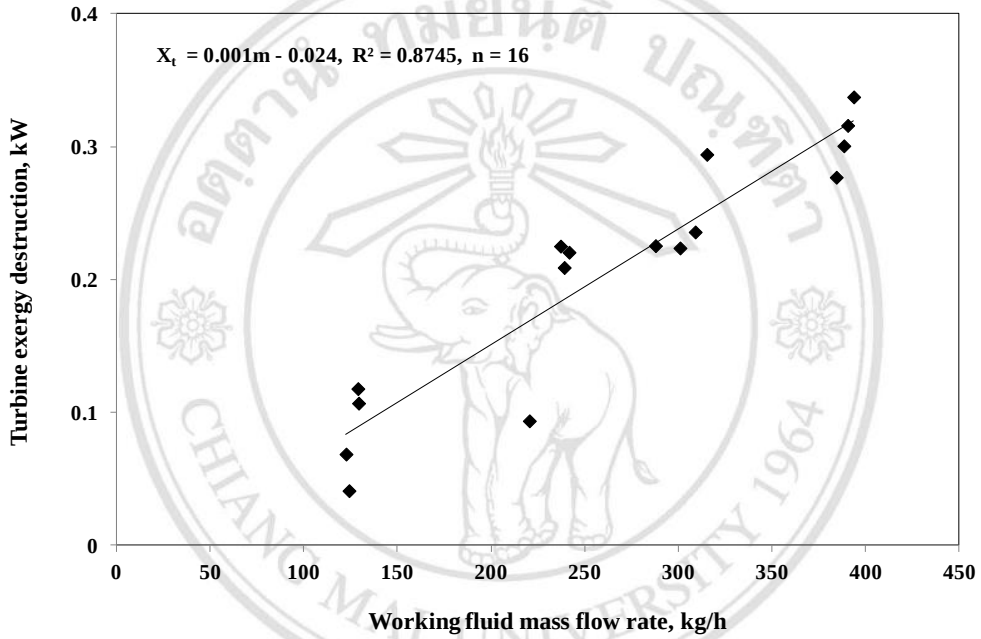

Figure 4.17: Turbine exergy destruction on working fluid mass flow rate

Figure 4.18 the system second law efficiency with the turbine inlet temperature for heat sources temperature of all experiments with the varied working fluid mass flow rate. The second-law efficiency increases for the entire working fluid mass flow rate with the increase of the turbine inlet temperature.

Figure 4.19 the effects of the turbine energy loss percentage with the turbine exergy destruction for heat source temperature and working fluid mass flow rates all experiment. The turbine exergy destruction increases for all the experiments with the increase of the turbine energy loss percentage. The results presented in Figure 4.19 indicate that the system will be more beneficial in system with annual low turbine

ลิขสิทธิ์มหาวิทยาลัยเชียงใหม่
Copyright© by Chiang Mai University
All rights reserved

exergy destruction, since the system will have good the first and second law efficiencies.

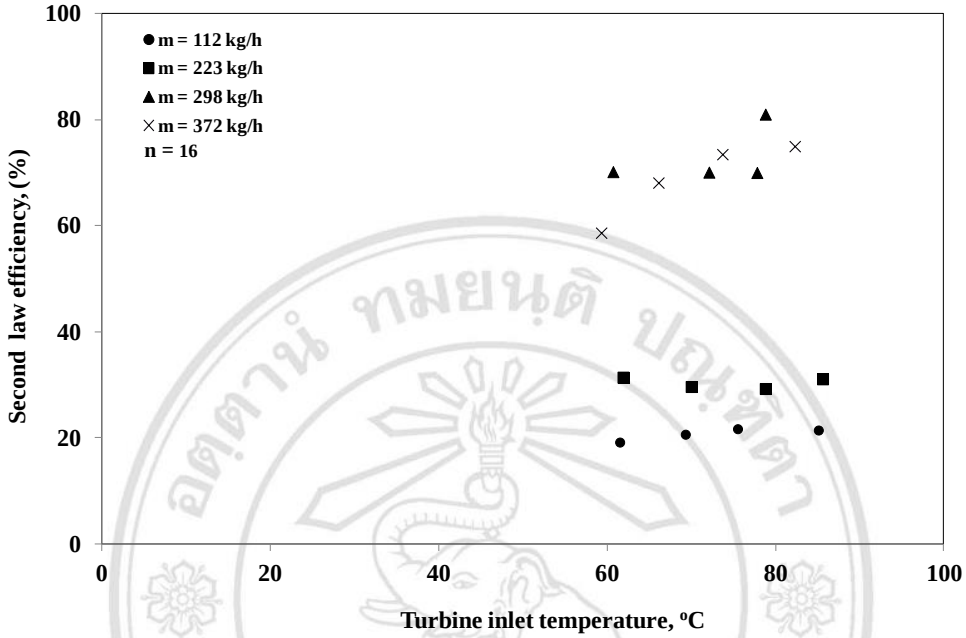

Figure 4.18: Second law efficiency on turbine inlet temperature

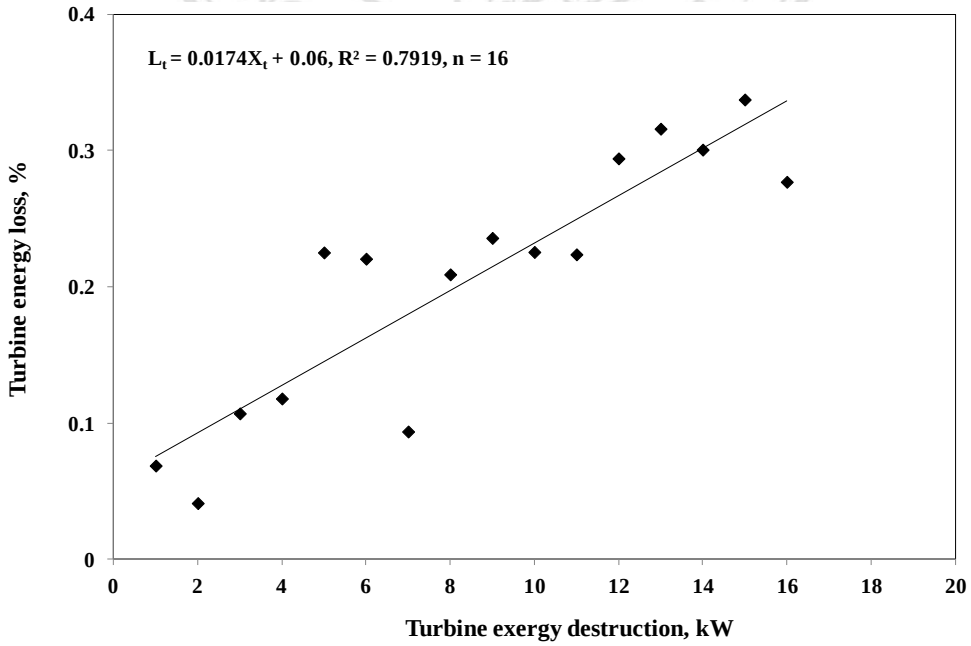

Figure 4.19: Effects of turbine energy loss percentage on turbine exergy destruction

The results in the Figures 4.17, 4.18 and 4.19 indicate that the low exergy destruction in ORC system will be more beneficial in the higher efficiencies. The low exergy destruction in system will be system performance increment was caused by lower destroyed of system.

4.3.3 Proportion of Thermodynamics Properties in Components

The Table 4.5 and 4.6, and Figure 4.20 and 4.21 shown the irreversibility, energy and exergy on the ORC system was determined. The table includes the following parameters, temperature, specific enthalpy, specific entropy, heat, work, and irreversibility associated with each of the components. The data for the flow parameter table were calculated using Microsoft Excel software. Using the information provided in the Tables 4.6, the vapor generator heat input rate, the condenser heat rejected rates, the working fluid mass flow rate, the pump power consumption, and the turbine power can be determined.

Table 4.5: Analysis of irreversibility on test rig

Experimental simulation results (case of m = 327 kg/h and T_{so} = 95.4 ^{o}C)							
Point	state	T	h	s	Q	W	I
		(^{o}C)	(kJ/kg)	(kJ/kgK)	(kW)	(kW)	(kW)
1	Pump	31.3	236.01	1.1246	-	0.048	0.41
2	Vapor generator	31.7	236.47	1.1262	23.73	-	8.64
3	Turbine	82.3	493.37	1.8612	-	0.319	0.28
4	Condenser	77.6	490.28	1.8600	21.25	-	4.89

Table 4.6: Analysis of performance in maximum heat source temperature and working fluid mass flow rate case

Components	Energy	Exergy
Vapor generator heat rate (kW)	23.733	8.638
Condenser Heat rejection (kW)	21.247	4.888
Turbine power (kW)	0.016	0.277
Pump power consumption (kW)	0.413	0.414
Net power output (kW)	0.397	-
Thermal efficiency (%)	0.07	-
Working fluid mass flow rate (kg/h)	372.2	-
Heat input temperature (^{o}C)	96.8	-
Heat rejection temperature (^{o}C)	11.2	-

ลิขสิทธิ์มหาวิทยาลัยเชียงใหม่
Copyright© by Chiang Mai University
All rights reserved

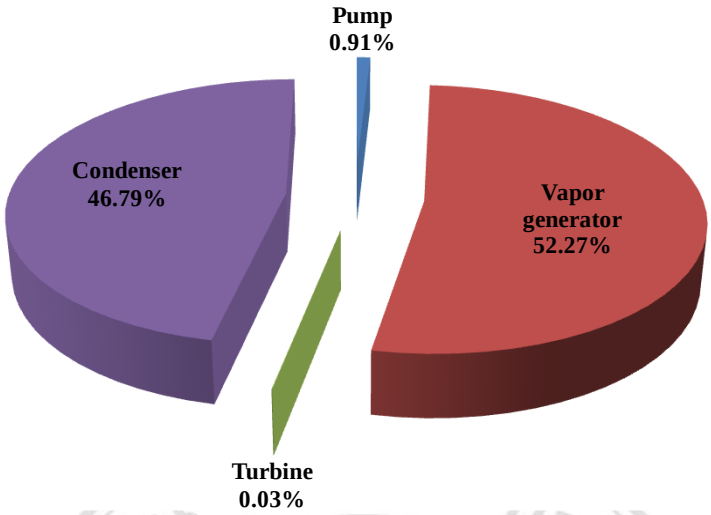

Figure 4.20: Proportion of energy used on system of maximum heat source temperature

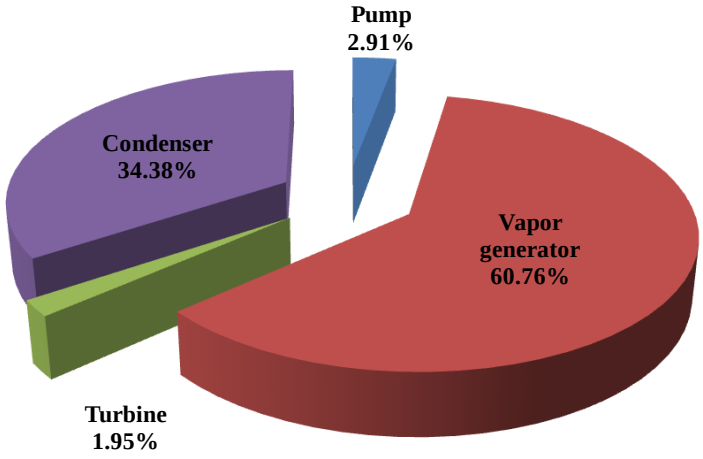

ลิขสิทธิ์มหาวิทยาลัยเชียงใหม่
Copyright© by Chiang Mai University
All rights reserved

Figure 4.21: Proportion of exergy on system of the maximum heat source temperature

4.3.4 Effects of Exergy Destruction on System

The numerical simulation results to determine the thermodynamic characteristics of the exergy destruction investigated each of components on system were analyzed. The Table 4.7 had shown the higher heat source temperature case which includes the following parameters, specific enthalpy difference, specific entropy difference, availability difference and irreversibility is presented.

Table 4.7: Thermodynamic characteristics of system on higher temperature heat source

Stage		Δh (kJ/kg)	Δs (kJ/kgK)	ΔΨ (kJ/kg)	X (kW)	X_{des} Percentage (%)
1	Pump	0.46	0.00152	0.000232	0.41	2.87
2	Vapor generator	256.90	0.73503	37.75	8.64	59.90
3	Turbine	3.09	0.00117	2.74	0.48	3.34
4	Condenser	253.11	0.73159	34.99	4.89	33.90
	Total				**14.42**	**100**

The results from Table 4.7 indicated that the vapor generator was the component that has the highest exergy losses 8.64 kW. Also, it was the component with the lowest efficiency 60%. The exergy destruction in the vapor generator is mainly due to the irreversibility associated with heat transfer and the exergy loss associated with the heat source temperature.

For this case, the exergy destruction percentage was about 60% of the initial exergy of the working fluid in the vapor generator. The high exergy destruction also causes a decrease in the degree of thermodynamic perfection, which shows its highest value in the vapor generator. On the other hand, the vapor generator was the component with the high influence coefficient, which reflects the fact that the vapor generator is the critical component of the evaluated system. The second component that has more influence on the system performance is the condenser. The condenser shows the second highest coefficient of influence about 34%. However, the degree of thermodynamic perfection and exergy efficiency were higher for the turbine component compared to the vapor generator.

ลิขสิทธิ์มหาวิทยาลัยเชียงใหม่
Copyright© by Chiang Mai University
All rights reserved

4.3.5 Effect of Working Fluid Mass Flow Rate on Exergy Destruction and Exergy Efficiency

Figure 4.22 showed the effects of the exergy efficiencies and total exergy destruction decreases with the working fluid mass flow rate on the system. The result was consistent, since a decrease of the total exergy destruction corresponds to an increase in the system exergy efficiency. This system due to the fact that when the vapor generator temperature was increased, the difference between the vapor generator

temperature and the heat source temperature input the vapor generator was reduced. The reduction in the temperature difference leads to an improvement of the exergy efficiency or a reduction of the system exergy destruction. For low inlet turbine pressures, the second law efficiencies for high-temperature heat source on system was approximately 0.12% higher than those obtained for low-temperature heat source on the system, while for high inlet turbine pressures the second law efficiencies for low-temperature heat source was approximately 0.03% lower than those obtained for high-temperature heat source on the system.

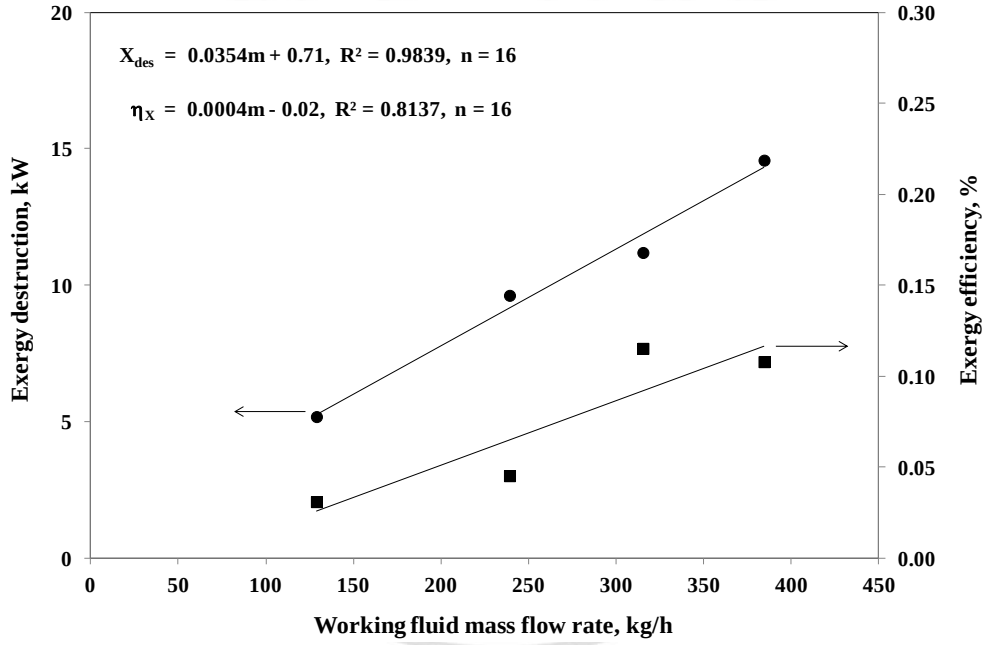

Figure 4.22: Effect of exergy destruction and exergy efficiency on working fluid mass flow rate

ลิขสิทธิ์มหาวิทยาลัยเชียงใหม่
Copyright© by Chiang Mai University
All rights reserved

4.3.6 Influence of Working Fluid on Power Output and Irreversibility

Figure 4.23 illustrated the effects of system power output and system irreversibility on the working fluid mass flow rate in the maximum heat source temperature fourth case. To generate this figure, the vapor generator temperature was kept at 90.0 – 97.2°C while the condenser temperature was kept at 10 - 12°C. The system receives heat from a heat source input at a rate of 54 kW at a constant mass flow rate of 327 kg/h. The heat source temperature was changed from 71.6 – 95.7°C. As

expected, the system efficiency remains constant for system with the increased of the heat source temperature. However, it was demonstrated that high-temperature heat source produces better thermal efficiencies than low-temperature heat source.

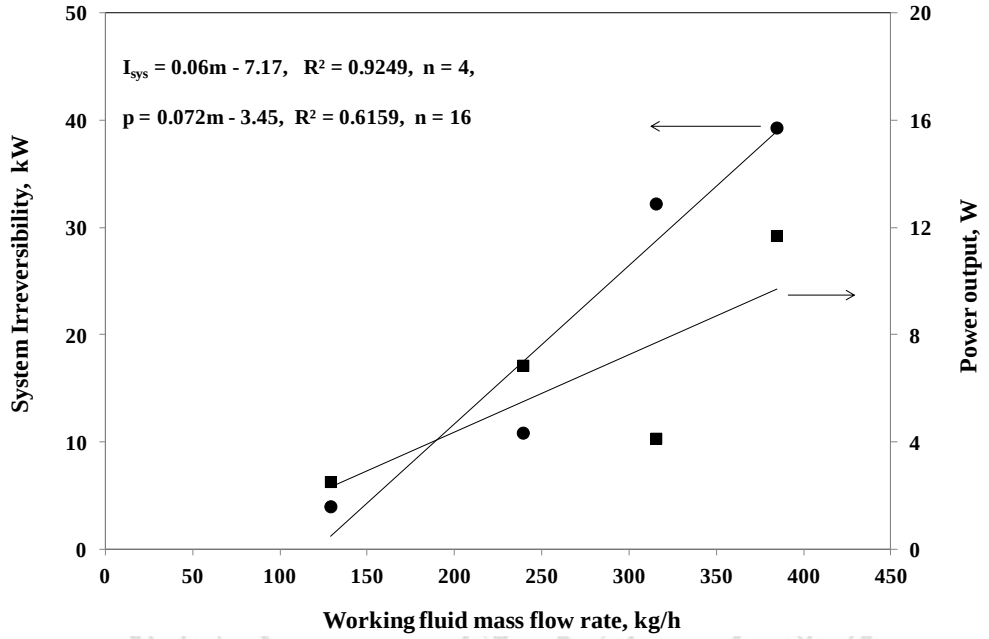

Figure 4.23: Power output and system irreversibility on working fluid mass flow rate in maximum heat source temperature case

4.4 Verification of Numerical and Experimental ORC system

The results that simulated for the system under the same conditions as those found experimentally, a comparison can now be made. The theoretical computations suggest that cycle efficiency between of 8.4 – 14.2% is achievable whereas the cycle efficiency of the experimental apparatus was 0.07 – 0.14%. This shows that the test rig was only able to achieve 0.37% of that theoretically projected for the experienced conditions and with the apparatus used.

4.4.1 Comparison of Overall Heat Transfer on Heat Source Temperature

The cycle parameters for a theoretical system have been calculated, using the same method as in Section 4.1, and are presented in Table 4.8.

ลิขสิทธิ์มหาวิทยาลัยเชียงใหม่
Copyright© by Chiang Mai University
All rights reserved

Table 4.8: Optimum condition of maximum working fluid mass flow rate test case

Numerical simulation and Experimental comparison	Optimum of the maximum working fluid mass flow rate case							
	Nu	Exp	Nu	Exp	Nu	Exp	Nu	Exp
Heat source temperature (°C)	70.0	71.0	80.0	84.1	90.0	91.8	100.0	96.8
Vapor generator inlet temperature (°C)	30.0	28.7	30.0	31.3	30.0	31.5	30.0	31.8
Vapor generator outlet temperature (°C)	60.0	61.1	70.0	69.1	80.0	75.4	90.0	85.1
Log-mean temperature difference (°C)	21.6	22.3	24.9	30.0	27.9	33.7	30.8	31.1
Average heat transfer coefficient (W/m^2°C)	287.3	209.3	256.9	180.0	234.8	178.7	217.8	207.0
Overall heat transfer coefficient (W/m^2°C)	768.5	401.5	687.2	374.9	628.1	355.7	582.6	369.1
Vapor generator heat transfer rate (kW)	13.5	13.0	18.0	17.3	22.6	20.2	27.1	23.7
Vapor generator effectivness (-)	0.75	0.77	0.80	0.72	0.83	0.73	0.86	0.82

Nu = numerical simulation results

Exp = experimental results

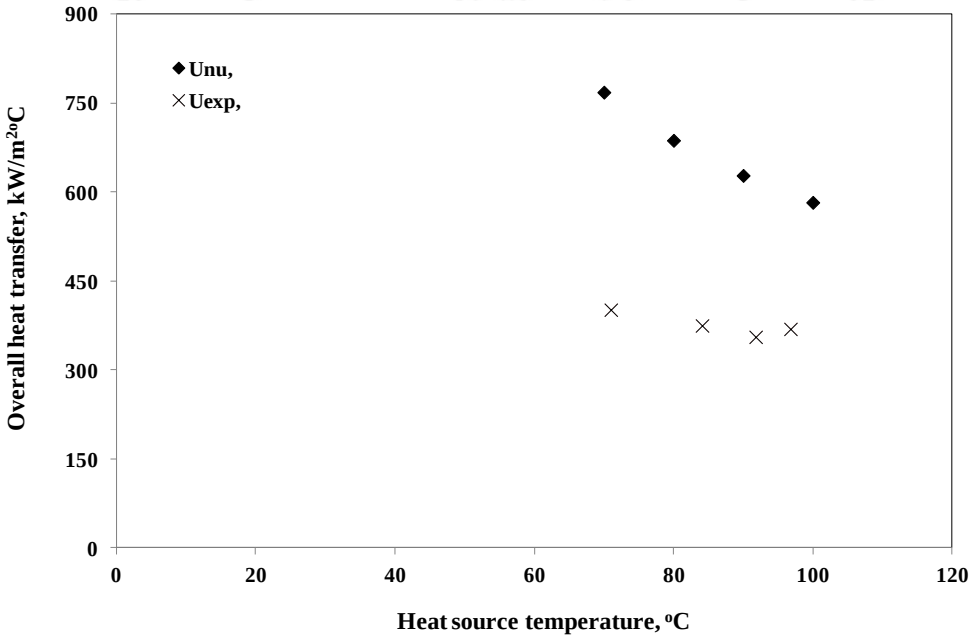

Figure 4.24: Effects of overall heat transfer on heat source temperature in optimum condition of working fluid mass flow rate 327 kg/h

The trends displayed in the Figure 4.24 illustrated effects of the overall heat transfer decreasing on the heat source temperature in the vapor generator. These are the outcome predicted by basic theory and experiment on system. What is also evident from the results was the decreasing net cycle efficiency of the experimental results when compared to the theoretical results. This trend line was most likely attributable to the operational characteristics of the turbine. The increased heat source temperature was likely to suit the geometry of the turbine and porting and thus be the cause of the relative increase in efficiency.

4.4.2 Comparison of Heat Transfer on Working Fluid Mass Flow Rate

The numerical and experimental results compared with the various heat source temperatures were provided below in Table 4.9. It should be noted that as the heat transfer rate in the system was increased, so too was the maximum working fluid mass flow rate. This was done to ensure that there was sensible heating only.

Table 4.9: Heat transfer on system on temperature heat source difference

Numerical simulation and experiment comparison	**Optimum of the maximum HCFC-141b mass flow rate testing case**							
	Nu	**Exp**	**Nu**	**Exp**	**Nu**	**Exp**	**Nu**	**Exp**
HCFC-141b mass flow rate (kg/h)	372.2	390.5	372.2	388.5	372.2	393.7	372.2	384.4
Heat source temperature at vapor generator (°C)	70.0	71.0	80.0	84.1	90.0	91.8	100.0	96.8
Cooling water temperature (°C)	10.0	11.4	10.0	11.4	10.0	11.3	10.0	11.2
High pressure side (kPa)	246.0	241.1	324.8	292.4	421.2	358.6	537.7	446.5
Low pressure side (kPa)	164.0	210.9	216.5	257.1	280.8	311.1	358.4	396.7
HCFC-141b vapor generator inlet temperature (°C)	30.3	32.1	30.3	29.6	30.3	31.7	30.3	31.7
HCFC-141b vapor generator outlet temperature (°C)	60.0	59.3	70.0	66.1	80.0	73.7	90.0	82.3
HCFC-141b condenser inlet temperature (°C)	46.5	54.7	55.7	61.5	64.7	68.4	73.3	77.6
HCFC-141b condenser outlet Temperature (°C)	30.0	31.4	30.0	31.2	30.0	30.8	30.0	32.3

Nu = numerical simulation results

Exp = experimental results

ลิขสิทธิ์มหาวิทยาลัยเชียงใหม่
Copyright© by Chiang Mai University
All rights reserved

The results give insight into the vapor generator performance in this system. As the heat source temperature was increased, the temperature difference between the heat source temperature and the working fluid mass flow rate in the vapor generator exit temperature increased at a rising rate. This indicates shows that heat transfer could be improved by using a larger heat exchanger for the vapor generator. A chart of the working fluid in the vapor generator outlet temperature as a function of heat source temperature is shown in Table 4.9.

4.4.3 Comparison of Energy and Exergy Efficiency in System

The numerical and experimental results for the investigated range of operating conditions are provided in Table 4.10. Also included in the table were the calculated values, pertaining to the efficiency of the rig, which have been calculated identically to those for the test detailed in Section 4.4.1 and using the fluid properties found in Appendix B.

Table 4.10: Performance results on heat source temperature difference

Numerical simulation and testing comparison	**Optimum of the maximum HCFC-141b mass flow rate testing case**							
	Nu	**Exp**	**Nu**	**Exp**	**Nu**	**Exp**	**Nu**	**Exp**
Pressure ratio	1.50	1.14	1.50	1.14	1.50	1.15	1.50	1.13
Turbine torque (N-m)	-	0.06	-	0.09	-	0.10	-	0.11
Power output (kW)	2.11	0.01	2.75	0.01	3.36	0.01	3.86	0.02
Turbine rotation speed (RPM)	-	965	-	1,095	-	1,229	-	1,369
Vapor generator heat transfer rate (kW)	13.48	12.96	18.02	17.30	22.56	20.18	27.10	23.73
Condenser heat transfer rate (kW)	7.51	11.10	11.66	14.36	15.74	18.06	19.66	21.25
Exergy destruction (kW)	-	7.92	-	10.15	-	28.88	-	14.22
Net overall efficiency (%)	15.66	0.05	15.25	0.06	14.87	0.06	14.25	0.07
Carnot cycle efficiency (%)	11.57	8.18	14.07	8.18	16.44	12.11	18.68	14.24
Exergy efficiency (%)	-	0.081	-	0.100	-	0.045	-	0.111

Nu = numerical simulation results

Exp = experimental results

ลิขสิทธิ์มหาวิทยาลัยเชียงใหม่
Copyright© by Chiang Mai University
All rights reserved

Figure 4.24 the results show that an increasing heat transfer rate of vapor generator with increasing heat source temperatures as was expected from the experiment. There is also a significant trend in the results, again expected, for increasing energy and exergy efficiency as the heat transfer rate of vapor generator and heat source temperature were increased. For this analysis, the power consumed by the heat source and heat sink of working fluids was considered to be the same for all tests. This value for the parasitic load, the net overall efficiency has been calculated and also shows an increased energy and exergy efficiency.

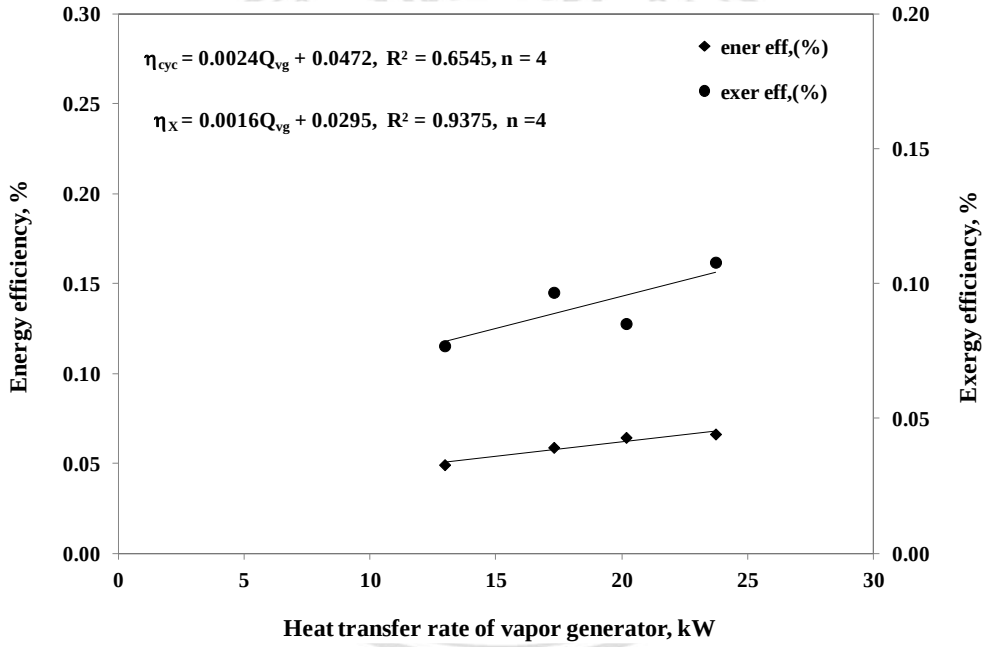

Figure 4.25: Energy and exergy efficiency on the heat rate of vapor generator

ลิขสิทธิ์มหาวิทยาลัยเชียงใหม่
Copyright© by Chiang Mai University
All rights reserved

The energy and exergy efficiencies of ORC from the experimental results as a function of the heat transfer rate of vaporgenerator and working fluid is illustrated in Figure 4.25. It displays a clear trend of increasing conversion efficiency with increasing the working fluid on the vapor generator temperature for both the energy and exergy efficiency calculations. This shows an increasing work ratio for an increased working fluid on vapor generator exit temperature as the overall efficiency approaches the cycle efficiency.

4.5 Conclusion

This chapter concluded the results have possibility of an ORC working with HCFC-141b as a working substance has been investigated, obtaining both numerical and experimental results. The numerical results shown that the optimum condition occurred when increase the high temperature heat source and the inlet turbine temperature over the boiling point of working fluid. If the working fluid latent heat has a low value, the optimum running condition was achieved. With regard to the rotation speed and power output of the turbine, it was shown that the working fluid can also improve the system performance. The conclusions are as follows

4.5.1 Development Methods on This System

1. Increasing in the order to the heat sources in the vapor generator. The mean temperature of the heat source. The vapor generator would be better if the heat source was to be found on the large exchange of the vapor generator. The temperature profile would be improved, and the energy losses would lower significantly.

2. Enhancement of the turbine. This point is probably the most central. As mentioned before, the turbine is not optimized. It is this component of the cycle that shows the highest prospective for development. The internal leaks may be condensed, as well as the exterior leaks that cause fluid losses. The abrasion torque may also be simply reduced.

3. The most favorable would be a radial turbine, which shows compensation: No peripheral leaks and thus no working fluid losses. This would then permit the utilization of a flammable working fluid, which has not used because of the leakage possibility and decrease heat losses, the power generating device if integrated into the turbine, its inefficiencies could result in heat that may be transmitted to the fluid. It is nonetheless imperative to put into practice a generating device capable of performance in a high range of temperatures. The lubrication of the radial turbine would also be valuable, as the leakage area and the friction torque could be reduced.

ลิขสิทธิ์มหาวิทยาลัยเชียงใหม่
Copyright© by Chiang Mai University
All rights reserved